

Nonlinear Power Method for Computing Eigenvectors of Proximal Operators and Neural Networks

Leon Bungert^{*§}, Ester Hait-Fraenkel^{†§}, Nicolas Papadakis[‡], and Guy Gilboa[†]

Key words. Nonlinear power method, Power iterations, Proximal operators, Neural networks

Abstract. Neural networks have revolutionized the field of data science, yielding remarkable solutions in a data-driven manner. For instance, in the field of mathematical imaging, they have surpassed traditional methods based on convex regularization. However, a fundamental theory supporting the practical applications is still in the early stages of development. We take a fresh look at neural networks and examine them via nonlinear eigenvalue analysis. The field of nonlinear spectral theory is still emerging, providing insights about nonlinear operators and systems. In this paper we view a neural network as a complex nonlinear operator and attempt to find its nonlinear eigenvectors. We first discuss the existence of such eigenvectors and analyze the kernel of ReLU networks. Then we study a nonlinear power method for generic nonlinear operators. For proximal operators associated to absolutely one-homogeneous convex regularization functionals, we can prove convergence of the method to an eigenvector of the proximal operator. This motivates us to apply a nonlinear method to networks which are trained to act similarly as a proximal operator. In order to take the non-homogeneity of neural networks into account we define a modified version of the power method. We perform extensive experiments on various shallow and deep neural networks designed for image denoising. For simple nets, we observe the influence of training data on the eigenvectors. For state-of-the-art denoising networks, we show that eigenvectors can be interpreted as (un)stable modes of the network, when contaminated with noise or other degradations.

1. Introduction. The emerging field of nonlinear spectral theory allows better understanding of nonlinear processes, as well as designing algorithms based on nonlinear spectral methods. In this paper, we make a first step towards understanding neural networks via their (nonlinear) eigenvectors. In image processing and learning, there were several theoretical advances in analyzing nonlinear eigenproblems. [32, 4] formulated analytic solutions for eigenfunctions associated to the 1-Laplacian. [5] analyzed properties of ground states of one-homogeneous functionals. A nonlinear spectral decomposition based on total-variation proposed in [22, 23] was later generalized to the one-homogeneous case in [12], with theory for the discrete case. Recently, [9, 10] rigorously analyzed this framework in the continuous setting. A p -Laplacian spectral framework is formulated in [16]. Applications to image denoising [34], segmentation [43], fusion [25] and classification [2] were proposed.

A very difficult problem for general nonlinear operators is how to compute their eigenvectors. In the context of learning, the authors of [41] estimated the Cheeger cut on graphs by a Rayleigh-type quotient. This was later generalized in [27] to a nonlinear inverse-power method. [36, 1, 7] suggested nonlinear flows to solve eigenproblems induced by total-variation and one-homogeneous functionals. This flow was later generalized to solve eigenproblems emerging in nonlinear optics [15]. Algorithms to minimize generalized Rayleigh-quotients on

^{*}Department of Mathematics, University of Erlangen (leon.bungert@fau.de)

[†]Department of Electrical Engineering, Technion - Israel Institute of Technology

[‡]Univ. Bordeaux, IMB, Bordeaux INP, CNRS, UMR 5251 F-33400 TALENCE, France

[§]These authors contributed equally to this work.

grids and graphs were proposed and analyzed in [20]. The methods above assume either that the operator is a subgradient of a convex functional, or at least an analytically known operator. Significantly more complex nonlinear operators were only recently studied for the first time, for the case of nonlinear denoisers, as suggested by part of the authors in [26]. We follow and generalize this direction for neural nets and provide a comprehensive analysis for nonlinear proximal operators.

Neural networks have revolutionized the world of computer vision and image processing [18], applied for many tasks, such as classification and segmentation (cf. [40] for an overview), depth estimation [30, 21], tracking [19, 35], to name a few. An ongoing extensive research on mathematical frameworks aims to interpret neural nets. This includes earlier studies in the context of wavelets and a generalization of the scatter transform [31], the interpretation of residual networks as nonlinear ODEs [24, 14], deep layer limits [42], sparse coding [37] and more. Recent studies, more closely related to our work, are the SVD analysis of a ReLU layer [17] and convergence of plug-and-play ADMM algorithms using denoising networks with certain Lipschitz regularity [39].

Similarly to many of the contributions above, we focus on nets with inputs and outputs of the same dimension. That is, given an input image, the output of the network is an image of the same size, which is common in many image-processing tasks. More specifically, although our algorithms are more general, we direct our efforts towards denoising networks (e.g. [44, 45]). Given a noisy image, such nets estimate a suitable clean image. In this setting a nonlinear eigenvalue problem can be well defined, along with some general regularity assumptions on the behavior of the net. Our main contributions are

1. We propose a generalization of the linear power method, a classical iterative method to compute eigenvectors of matrices.
2. We provide a rigorous analysis of the method for a certain class of nonlinear proximal operators, showing its validity.
3. We discuss existence of eigenvectors of neural nets and characterize the kernel of ReLU nets as convex polyhedra.
4. By computing eigenvectors of state-of-the-art denoising networks we gain insights on the most and least stable structures of the net.

2. Setting and Definitions. Let $T : \mathcal{H} \rightarrow \mathcal{H}$ be a generic (nonlinear) operator on a real Hilbert space \mathcal{H} with norm $\|\cdot\|$. In the case of a neural network one typically has $\mathcal{H} = \mathbb{R}^n$, equipped with the Euclidean norm. We aim at solving the generalized *nonlinear* eigenproblem

$$(2.1) \quad T(u) = \lambda u,$$

where $u \in \mathcal{H}$ and $\lambda \in \mathbb{R}$ denote the eigenvector and eigenvalue, respectively.

Rayleigh quotient. A common notion in linear eigenvalue analysis is the Rayleigh quotient [29], defined for symmetric matrices L as:

$$(2.2) \quad R_{\text{lin}}(u) := \frac{u^T L u}{u^T u} = \frac{\langle u, L u \rangle}{\|u\|^2}.$$

The Euler-Lagrange equation of (2.2) results in the eigenproblem. Therefore, an eigenvector is a critical point of the Rayleigh quotient. We can also understand the Rayleigh quotient as

a generalized or approximated eigenvalue for any u (not just eigenvectors). For eigenvectors (admitting (2.1)), we get exactly the corresponding eigenvalue $R(u) = \lambda$. The Rayleigh quotient can be generalized in the nonlinear setting to a *generalized Rayleigh quotient*,

$$(2.3) \quad R(u) = \frac{\langle u, T(u) \rangle}{\|u\|^2}.$$

When $T(u)$ is a subgradient of an absolutely one-homogeneous functional J , meaning $T(u) \in \partial J(u)$, we have $J(u) = \langle u, T(u) \rangle$. In this case (2.3) becomes (see [36]) $R(u) = J(u)/\|u\|^2$ and the eigenvalue problem takes the form $\lambda u \in \partial J(u)$. In [28] similar quotients were used to obtain an inverse-power method. In [20, 7] the minimization of such quotients based on one-homogeneous functionals were analyzed and used to solve eigenvalue problems.

Approximate eigenvectors and angle. Another important concept related to numerical solutions of eigenvectors is their approximation. In nonlinear systems one may often reach only an approximation of an eigenvector. We would like to quantify how close a given vector is to a precise eigenvector. One general formulation for any operator T , is by the angle (see [36]). For eigenvectors, vectors u and $T(u)$ are collinear. Thus their respective angle is either 0 (for positive eigenvalues) or π (for negative eigenvalues). Since both u and $T(u)$ are real, eigenvalues are also real. Thus, the angle is a simple scalar measure that quantifies how close u and $T(u)$ are to collinearity. We define the angle θ between u and $T(u)$ by

$$(2.4) \quad \cos(\theta) = \frac{\langle u, T(u) \rangle}{\|u\| \|T(u)\|}.$$

We discuss denoisers with positive eigenvalues, thus we aim to reach an angle close to 0.

Linear Power Method. We briefly recall the linear power method algorithm (also known as Von-Mises-iteration [33]), which we generalize in this work. Given a matrix $L \in \mathbb{R}^{n \times n}$ which is diagonalizable, the linear eigenproblem is

$$(2.5) \quad Lu = \lambda u.$$

A solution to this problem is found by the iterative algorithm given in [Algorithm 2.1](#). Under some conditions the algorithm converges to the eigenvalue λ with the greatest absolute value, and to its corresponding eigenvector.

Algorithm 2.1 *Linear Power Method with Matrix L*

Input: $f \in \mathbb{R}^n$, $\varepsilon > 0$.

1. Initialize: $u^0 \leftarrow f/\|f\|$, $k \leftarrow 1$.
2. Repeat until $\|u^{k+1} - u^k\| < \varepsilon$:
 $u^{k+1} \leftarrow \frac{Lu^k}{\|Lu^k\|}$, $k \leftarrow k + 1$.

Output: (u^*, λ^*) , where $u^* = u^k$, $\lambda^* = R(u^*)$, with R defined in (2.2).

3. Networks as Nonlinear Operators - Existence of Eigenvectors and Kernel. In this section, we first aim at proving existence of eigenvectors for a generic class of nonlinear operators, including most neural nets. Using Banach's fixed point theorem we will see that

Lipschitz continuity suffices to prove existence of eigenvectors. Secondly, we study a special class of eigenvectors, namely vectors in the kernel of the operator which fulfill (2.1) with $\lambda = 0$, by definition. These eigenvectors are of special interest since they characterize the most unstable inputs to the neural net. For example, if the net is supposed to denoise images then the kernel can be interpreted as pure noise images. While for linear operators and also for subdifferential operators of homogeneous functionals the kernel can be shown to be a linear space [7, 9], this is not true for general nonlinear operators. In order to develop a first understanding of the kernel of neural nets we characterize the kernel of ReLU networks in the single- and multi-layer case.

3.1. Existence of eigenvectors. In order to prove existence of eigenvectors we consider T as an operator $T : U \rightarrow U$, where $U \subset \mathcal{H}$ is some closed subset of \mathcal{H} which meets

$$(3.1) \quad cU \subset U, \quad \forall 0 \leq c \leq 1.$$

Relevant examples for neural nets are the non-negative orthant $U = \mathbb{R}_+^n$, the unit cube $U = [0, 1]^n$, or the whole space $U = \mathbb{R}^n$. The infinite-dimensional counterparts of these examples are L^2 -functions which take only non-negative values or values in $[0, 1]$. Our only assumption on the operator T is that it is Lipschitz continuous with some constant $L > 0$, meaning

$$(3.2) \quad \|T(u) - T(v)\| \leq L \|u - v\|, \quad u, v \in U.$$

Proposition 3.1. *Under the assumptions (3.1) and (3.2), operator T has an eigenvector, i.e., there exists $u^* \in U$ and $\lambda > 0$ such that $T(u^*) = \lambda u^*$.*

Proof. The proof uses Banach's fixed point theorem. If T is Lipschitz continuous with constant $L < 1$, then T is a contraction and hence has a unique fixed point $u^* \in U$ satisfying $T(u^*) = u^*$.

If the Lipschitz constant L of T is greater or equal than 1, we define a new map $T_\varepsilon := T/(L + \varepsilon)$ for $\varepsilon > 0$, which is a contraction. Furthermore, T_ε maps U into U by the assumption that $cU \subset U$ for $0 < c \leq 1$. Hence, reasoning as above, there exists a unique $u^* \in U$ such that $T_\varepsilon(u^*) = u^*$, which can be rewritten as $T(u^*) = (L + \varepsilon)u^*$. ■

Remark 3.1. *The main drawback of the result above is that one cannot assure that the eigenvector, whose existence is proved, is different from zero. For instance, if it is known that $T(0) = 0$ then 0 is the unique fixed point of T_ε .*

Hence, in order to show that a given neural net T has an eigenvector, we simply have to make sure T is Lipschitz continuous. This, however, is fulfilled for most networks types.

Example 3.2 (Deep neural nets). *Deep neural nets of the form*

$$(3.3) \quad T(u) = \sigma(A^{(n)}) \dots \sigma(A^{(2)}) \sigma(A^{(1)}u + b^{(1)}) + b^{(2)} \dots + b^{(n)}, \quad u \in \mathbb{R}^n,$$

with weight matrices $A^{(k)} \in \mathbb{R}^{n \times n}$ and bias vectors $b^{(k)} \in \mathbb{R}^n$ for $k = 1, \dots, n$ are Lipschitz continuous if the activation function σ is Lipschitz continuous. For most popular choices of σ (such as ReLU, TanH, Logistic, SoftPlus, etc.) this is fulfilled.

3.2. The Kernel of ReLU Networks. As mentioned before we now study the kernel of T , which is given by

$$(3.4) \quad \ker(T) := \{u \in \mathcal{H} : T(u) = 0\}.$$

In the following we study the case where T is a single-layer neural network with ReLU activation and sketch how to extend this for multi-layer networks. The fundamental difference between these two cases is that, in general, the kernel is a convex cone for single-layer networks and, more generally, a convex polyhedron in the multi-layer case.

3.2.1. Single-layer case. We consider a single-layer network of the form

$$(3.5) \quad T(u) = \sigma(Au + b), \quad u \in \mathbb{R}^n,$$

where $A \in \mathbb{R}^{n \times n}$ is a square weight matrix, $b \in \mathbb{R}^n$ denotes a bias vector, and σ is some activation function with $\sigma(x) = 0$ for $x \leq 0$, the prototypical example being

$$(3.6) \quad \sigma(x) = \text{ReLU}(x) = \max(x, 0)$$

or any smoothed version of it. Hence, the kernel of T can be written as

$$(3.7) \quad \ker(T) = \{u \in \mathbb{R}^n : Au + b \leq 0\},$$

where the inequality should be understood component-wise. We will make one assumption on the weights and biases which allows us to characterize the kernel explicitly. Without this assumption weaker versions of our results remain true.

Assumption 1 (Range condition). *We assume that $b \in \text{ran}(A)$.*

For the following statements, we need the notion of a convex cone with tip.

Definition 3.2. *A set $C \subset \mathbb{R}^n$ is called convex cone with tip $v_0 \in \mathbb{R}^n$ if $u + \alpha(u - v_0) \in C$ for all $u \in C$ and $\alpha \geq 0$. C is called polyhedral if it can be written as $C = \{u + v_0 \in \mathbb{R}^n : Mu \geq 0\}$ with some matrix $M \in \mathbb{R}^{n \times n}$.*

The following lemma states that preimages under affine maps preserve convex cones with tips and polyhedrality.

Lemma 3.3. *Let $C \subset \mathbb{R}^n$ be a convex cone with tip $v_0 \in \mathbb{R}^n$ and $F : \mathbb{R}^n \rightarrow \mathbb{R}^n$, $u \mapsto Au + b$, be an affine map. If there is $u_0 \in \mathbb{R}^n$ meeting $F(u_0) = v_0$, then $D := \text{preim}_F(C)$ is a convex cone with tip u_0 . Furthermore, if $C = \{u + v_0 \in \mathbb{R}^n : Mu \geq 0\}$ is polyhedral, so is D and it holds $D = \{u + u_0 \in \mathbb{R}^n : MAu \geq 0\}$.*

Proof. We take an element $u \in D = \text{preim}_F(C)$, meaning that $F(u) \in C$. We have to show that $u_\alpha := u + \alpha(u - u_0) \in D$ for any $\alpha \geq 0$. To this end we compute

$$\begin{aligned} F(u + \alpha(u - u_0)) &= A(u + \alpha(u - u_0)) + b = Au + \alpha Au - \alpha Au_0 + b \\ &= Au + b + \alpha(Au + b - (Au_0 + b)) = F(u) + \alpha(F(u) - F(u_0)) \\ &= F(u) + \alpha(F(u) - v_0) \in C, \end{aligned}$$

which follows since $F(u) \in C$ and C is a cone with tip v_0 . Hence, we have established $u_\alpha \in D$. For the second statement we assume that C is polyhedral and obtain

$$\begin{aligned} D &= \text{preim}_F(C) = \{u \in \mathbb{R}^n : F(u) \in C\} = \{u \in \mathbb{R}^n : F(u) = v + v_0, Mv \geq 0\} \\ &= \{u + u_0 \in \mathbb{R}^n : Au + F(u_0) = v + v_0, Mv \geq 0\} \\ &= \{u + u_0 \in \mathbb{R}^n : MAu \geq 0\}, \end{aligned}$$

where we again used $F(u_0) = v_0$. This shows that D is polyhedral and concludes the proof. ■

Applying these insights to the kernel (3.7) of the ReLU network T , one obtains

Theorem 3.3 (Kernel of a single-layer ReLU network). *Under Assumption 1 the kernel of T is a polyhedral convex cone with tip u_0 where $Au_0 = -b$. Furthermore, it holds*

$$(3.8) \quad \ker(T) = \{u + u_0 \in \mathbb{R}^n : -Au \geq 0\}.$$

Proof. For the proof one applies the statements above to the affine map $F(u) = Au + b$ and the polyhedral convex cone $C = \{u \in \mathbb{R}^n : u \leq 0\}$ with tip $v_0 = 0$. This cone can be written as $C = \{u \in \mathbb{R}^n : Mu \geq 0\}$ where $M := -\mathbb{I}$ denotes the negative identity matrix. ■

Remark 3.4 (Other activation functions). *If one considers activation functions which fulfill $\sigma(x) = 0$ if and only if $x = 0$, the discussion of the kernel becomes trivial. Either the equation $Au = -b$ has at least one solution, in which case the kernel is a single point or an affine space, or it does not, in which case the kernel is empty.*

3.2.2. Multi-layer case. Now we sketch how the kernel of a deep network can be obtained. For simplicity, we restrict ourselves to the case of two layers and consider

$$(3.9) \quad T(u) = \sigma(F^{(1)}(\sigma(F^{(2)}(u))))), \quad u \in \mathbb{R}^n,$$

where $F^{(k)}(u) = A^{(k)}u + b^{(k)}$ for $k = 1, 2$, denote the corresponding affine functions. We assume that there is an element u_0 which meets $A^{(2)}u_0 = -b^{(2)}$ and obtain

$$C^{(2)} := \text{preim}_{F^{(2)}}(\mathbb{R}_-^n) = \{u + u_0 \in \mathbb{R}^n : -A^{(2)}u \geq 0\}$$

from Theorem 3.3. This implies

$$\ker(T) = \{u \in \mathbb{R}^n : F^{(2)}(\sigma(F^{(1)}(u))) \leq 0\} = \{u \in \mathbb{R}^n : \sigma(F^{(1)}(u)) \in C^{(2)}\}.$$

At this point one cannot simply take the preimage of $C^{(2)}$ under $F^{(1)}$ to obtain the kernel of T , since the activation function σ is in the way. However, for ReLU-type activation functions one can simplify this to

$$(3.10) \quad \ker(T) = \text{preim}_{F^{(1)}}\left(C_+^{(2)}\right)$$

where $S_+ := \{\max(u, 0) : u \in S\}$ denotes the positive part of a set $S \subset \mathbb{R}^n$. Note than one can write $C_+^{(2)}$ as intersection of two polyhedral cones $C_+^{(2)} = C^{(2)} \cap \mathbb{R}_+^n$, which is a polyhedron, i.e., an intersection of finitely many half-spaces. Hence, the kernel is given by the preimage of the polyhedron $C_+^{(2)}$ under the affine map $F^{(1)}$ which is again a polyhedron, according to [46]. We condense these insights into

Theorem 3.5 (Kernel of a multi-layer ReLU network). *Let $T : \mathbb{R}^n \rightarrow \mathbb{R}^n$ be a multi-layer neural net with ReLU activation, given by (3.3). Then $\ker(T)$ is a (possibly unbounded) convex polyhedron.*

Remark 3.6 (Deep networks with multiple layers). *Note that for deep networks the kernel is found by taking successive preimages of non-negative polyhedra under affine maps and keeping only the positive parts. Hence, the kernel will in general be smaller the larger the numbers of layers is. In particular, if one of the preimages does not intersect the positive orthant, the kernel will be empty.*

4. Analysis of the Nonlinear Power Method. As a first step towards computing eigenvectors of neural nets, we study [Algorithm 4.1](#) below, which is a straightforward generalization of [Algorithm 2.1](#) to the nonlinear case, first studied in [26]. We first repeat some key results from [26]. Then, we analyze the algorithm for a specific family of nonlinear denoisers, which are proximal operators based on convex, absolutely one-homogeneous regularizers (such as total variation [13] and total generalized variation [6]). We will prove that the proximal power method converges to an eigenvector under natural assumptions. For numerical results with respect to the proximal operator of total variation we refer to [26]. Note that these homogeneous regularizers are not sensitive to the range of the vectors. However, we will present a toy example of a non-homogeneous single-layer ReLU net, showing the limitations of the standard power method and motivating the generalized method defined in [section 5](#).

4.1. A Simple Nonlinear Power Method. We define the following nonlinear power-iteration algorithm, to which we refer as a *simple* algorithm. This is an immediate generalization of [Algorithm 2.1](#), replacing the linear matrix L by a nonlinear operator $T(\cdot)$.

Algorithm 4.1 *Simple Power Method with Generic Operator T*

Input: $f \in \mathcal{H}$, $\varepsilon > 0$.

1. Initialize: $u^0 \leftarrow f/\|f\|$, $k \leftarrow 1$.
2. Repeat until $\|u^{k+1} - u^k\| < \varepsilon$:

$$u^{k+1} \leftarrow \frac{T(u^k)}{\|T(u^k)\|}, \quad k \leftarrow k + 1.$$

Output: (u^*, λ^*) , where $u^* = u^k$, $\lambda^* = R(u^*)$, with R defined in (2.3).

For [Algorithm 4.1](#) to be well defined, we assume that for all $k \in \mathbb{N}$ it holds $T(u^k) \neq 0$. For proximal operators this can be shown to be true (cf. [subsection 4.2](#) below). In the following propositions we recall some key properties of [Algorithm 4.1](#) from [26].

Proposition 4.1. *Algorithm 4.1 converges after a finite number of steps, i.e, there is $N \in \mathbb{N}$ such that for all $k > N$ it holds $u^{k+1} = u^k$ **if and only if** u^k solves the eigenproblem (2.1).*

Proposition 4.2.

1. For every $k \in \mathbb{N}$, $|R(u^k)| \leq \|T(u^k)\|$. This holds in equality **if and only if** u^k solves the eigenproblem (2.1).
2. If exactly at iteration $k = N$ [Algorithm 4.1](#) converged, then for all $k < N$, $|R(u^k)| < \|T(u^k)\|$, and for all $k \geq N$, $|R(u^k)| = \|T(u^k)\|$.

Proposition 4.3. *The angle between u^k and $T(u^k)$ is πn for $n \in \mathbb{Z}$ if and only if u^k solves the eigenproblem (2.1).*

In our numerical experiments a Rayleigh quotient which reaches a constant value serves as a good indication for convergence to an eigenvector. For the operators tested, the Rayleigh quotient approximately increases to the eigenvalue, however, a general proof for this is pending. As discussed in section 2, we also aim to reach an angle (2.4) close to 0, which will serve as our validation measure. Hence, we define

Definition 4.4. *We call u an approximate (positive) eigenvector of T if the angle θ given by (2.4) meets $0 < \theta < 0.5^\circ$ ($1^\circ = \pi/180$).*

We now examine the behavior of Algorithm 4.1 in two different cases. On one hand, we prove its convergence to a non-trivial eigenvector for proximal operators. On the other hand, we present a very simple toy example for the far more complex, non-homogeneous neural network, for which Algorithm 4.1 is not able to produce meaningful eigenvectors.

4.2. Analysis of a Proximal Power Method. In this section we analyse a nonlinear power method associated to the proximal operator of a convex functional. Let $J : \mathcal{H} \rightarrow \mathbb{R} \cup \{\infty\}$ be an absolutely one-homogeneous, convex, and lower semi-continuous functional, defined on a Hilbert space \mathcal{H} . Absolute one-homogeneity means that for all $u \in \mathcal{H}$ and numbers $c \neq 0$

$$(4.1) \quad J(cu) = |c|J(u), \quad J(0) = 0.$$

For detailed properties of such functionals see [9, 12]. The proximal operator of J is given by

$$(4.2) \quad \text{prox}_\alpha^J(u) := \arg \min_{v \in \mathcal{H}} \frac{1}{2} \|v - u\|^2 + \alpha J(v),$$

where $f \in \mathcal{H}$ and $\alpha \geq 0$ denotes the regularization parameter. A prototypical example for J is given by the total variation, defined on the Hilbert space $\mathcal{H} = L^2(\Omega)$ by setting

$$(4.3) \quad J(u) = \sup \left\{ \int_\Omega u \operatorname{div} \phi \, dx : \phi \in C_c^\infty(\Omega), \|\phi\|_\infty \leq 1 \right\}, \quad u \in L^2(\Omega).$$

In this case the proximal operator (4.2) coincides with the solution of the famous Rudin-Osher-Fatemi model [38]. We will now analyze Algorithm 4.1 with the nonlinear operator

$$(4.4) \quad T(u) = \text{prox}_{\alpha(u)}^J(u).$$

Here $\alpha(u)$ denotes regularization parameters which are allowed to depend on u . Constant parameters can be considered by setting $\alpha(u) \equiv \alpha > 0$. For the analysis we also introduce

$$(4.5) \quad \mathcal{N}(J) = \{u \in \mathcal{H} : J(u) = 0\},$$

which is referred to as null-space of J and indeed is a linear space [8]. An assumption which does not restrict generality but simplifies the notation is that one considers the proximal operator (4.2) acting on $u \in \mathcal{N}(J)^\perp$ only. Here $\mathcal{N}(J)^\perp$ denotes the orthogonal complement of the null-space. This is due to the fact that it holds

$$(4.6) \quad \text{prox}_\alpha^J(u) = \text{prox}_\alpha^J(u - \bar{u}) + \bar{u},$$

where $\bar{u} \in \mathcal{N}(J)$ denotes the orthogonal projection of $u \in \mathcal{H}$ onto $\mathcal{N}(J)$. Furthermore, $\text{prox}_\alpha^J(u) \in \mathcal{N}(J)^\perp$ if $u \in \mathcal{N}(J)^\perp$. If, for example, J equals the total variation, then the null-space consists of constant functions and its orthogonal complement is given by all zero-mean functions. In this case, the proximal operator is invariant under the mean value \bar{u} its input $u \in L^2(\Omega)$.

To show convergence of power method associated to the operator T in (4.4), we need two standing assumptions on the interplay between the functional J and the Hilbert norm $\|\cdot\|$.

Assumption 2 (Poincaré inequality). *There is a constant $c_P > 0$ such that $c_P \|u\| \leq J(u)$ for all $u \in \mathcal{N}(J)^\perp$.*

Assumption 3 (Compact sub-level sets). *The sub-level sets of $\|\cdot\| + J(\cdot)$ are compact.*

Example 4.1. *A relevant example where Assumption 2 and Assumption 3 are fulfilled is $J(u) = \|\nabla u\|_p$, where $p \in \left(\frac{2n}{n+2}, \infty\right]$ and $\Omega \subset \mathbb{R}^n$ is a bounded Lipschitz domain with $n \geq 2$ (cf. [7] and [11] for $p = \infty$). Note that in the relevant case that J equals the total variation (4.3) the assumptions hold true only in dimension $n = 1$, since the compact embedding $\text{BV}(\Omega) \Subset L^2(\Omega)$ exists only in one dimension. In two dimensions the embedding is only continuous and in higher dimensions it does not even exist. However, by demanding additional regularity for the initial condition u^0 of the power method, as for instance $u^0 \in L^\infty(\Omega)$, one can show that Assumption 2 and Assumption 3 hold true along the sequence which is generated by the iteration (cf. [9]).*

Example 4.2. *If \mathcal{H} is finite-dimensional and J is norm on a subspace of \mathcal{H} , then both assumptions are met due to the equivalence of norms in finite dimensions.*

In the following, we will need an important result (see for instance [3]) which characterizes the subdifferential of absolutely one-homogeneous functionals

Proposition 4.5 (Subdifferential). *Let $J : \mathcal{H} \rightarrow \mathbb{R} \cup \{\infty\}$ be convex and absolutely one-homogeneous. Then its subdifferential in $u \in \mathcal{H}$ is given by*

$$(4.7) \quad \partial J(u) = \{p \in \mathcal{H} : \langle p, v \rangle \leq J(v), \forall v \in \mathcal{H}, \langle p, u \rangle = J(u)\}.$$

Our first result characterizes the maximal regularization parameter $\alpha(u)$ in (4.4) such that the power method Algorithm 4.1 is well-defined.

Proposition 4.6. *For $u \in \mathcal{N}(J)^\perp$ it holds that $T(u) = \text{prox}_{\alpha(u)}^J(u) = 0$ if and only if $\alpha(u) \geq \|u\|_*$ where*

$$(4.8) \quad \|u\|_* := \sup_{p \in \mathcal{N}(J)^\perp} \frac{\langle u, p \rangle}{J(p)} \geq \frac{\|u\|^2}{J(u)}.$$

Furthermore, equality holds in (4.8) if and only if u is an eigenvector of ∂J , meaning $\lambda u \in \partial J(u)$ for $\lambda = J(u)/\|u\|^2$.

Proof. The first claim was proved in [8] and we just show the second one. By choosing $p = u$ in the supremum one always has $\|u\|_* \geq \|u\|^2/J(u)$. If u is an eigenvector there is $\lambda \geq 0$ such that $\lambda u \in \partial J(u)$. Using Proposition 4.5 we can draw two conclusions. First of all,

it holds $\langle \lambda u, u \rangle = J(u)$ and hence $\lambda = J(u)/\|u\|^2$. Secondly, one has $\langle \lambda u, p \rangle \leq J(p)$ for all $p \in \mathcal{H}$ which implies

$$\|u\|_* = \sup_{p \in \mathcal{N}(J)^\perp} \frac{\langle u, p \rangle}{J(p)} = \frac{1}{\lambda} \sup_{p \in \mathcal{N}(J)^\perp} \frac{\langle \lambda u, p \rangle}{J(p)} \leq \frac{1}{\lambda} = \frac{\|u\|^2}{J(u)},$$

such that $\|u\|_* = \|u\|^2/J(u)$. Conversely, if $\|u\|_* = \|u\|^2/J(u)$ then one obtains

$$\langle \lambda u, v \rangle = \lambda J(v) \frac{\langle u, v \rangle}{J(v)} \leq \lambda J(v) \|u\|_* = J(v), \quad \forall v \in \mathcal{H},$$

for $\lambda = J(u)/\|u\|^2$. Hence, $\lambda u \in \partial J(u)$. ■

Corollary 4.7 (Well-definedness of the power method). *Let $\alpha(u)$ in (4.4) satisfy*

$$(4.9) \quad \alpha(u) < \|u\|_*$$

Then for all initial conditions $f \in \mathcal{N}(J)^\perp$ the power method [Algorithm 4.1](#) is well-defined.

Proof. By [Proposition 4.6](#) we know that $T(u^k) = \text{prox}_{\alpha(u^k)}^J(u^k) \neq 0$ if and only if $\alpha(u^k) < \|u^k\|_*$. Hence $u^{k+1} \leftarrow T(u^k)/\|T(u^k)\|$ in [Algorithm 4.1](#) is well-defined. ■

Next, we show that the functional values $J(u^k)$ decrease along [Algorithm 4.1](#). This will be the key ingredient for convergence of the algorithm and follows from

Proposition 4.8 (Decrease of the Rayleigh quotient). *Let $u \in \mathcal{N}(J)^\perp \cap \text{dom}(J) \setminus \{0\}$, $v := \text{prox}_{\alpha(u)}^J(f)$, and $\alpha(u) < \|u\|_*$. Then it holds*

$$(4.10) \quad \frac{J(v)}{\|v\|} \leq \frac{J(u)}{\|u\|}$$

with equality if and only if $\lambda u \in \partial J(u)$ for $\lambda = J(u)/\|u\|^2$.

Proof. The optimality of v means that

$$\frac{1}{2} \|v - u\|^2 + \alpha(u)J(v) \leq \frac{1}{2} \|w - u\|^2 + \alpha(u)J(w), \quad \forall w \in \mathcal{H},$$

with equality if and only if $w = v$, due to the strict convexity of the objective functional. We define $w := \frac{\|v\|}{\|u\|}u$ which meets

$$\|w - u\|^2 = \|w\|^2 - 2\langle w, u \rangle + \|u\|^2 = \|v\|^2 - 2\|v\|\|u\| + \|u\|^2 \leq \|v - u\|^2.$$

Plugging this into the optimality above yields

$$\alpha(u)J(v) \leq \alpha(u)J(w) = \alpha(u) \frac{\|v\|}{\|u\|} J(u).$$

From [Proposition 4.6](#) we infer that $v \neq 0$. Hence, we can divide by $\|v\|$, cancel $\alpha(u)$, and arrive at the assertion. Equality holds if and only if

$$v = w = \frac{\|v\|}{\|u\|}u = cu$$

where $c := \|v\| / \|u\| > 0$. The optimality condition for problem (4.2) is given by

$$\frac{u - v}{\alpha(u)} \in \partial J(v).$$

Plugging in the expression for v yields

$$\frac{1 - c}{\alpha(u)} u \in \partial J(u),$$

where we used that $\partial J(v) = \partial J(cu) = \partial J(u)$ since $c > 0$ and J is absolutely one-homogeneous (cf. [9]). Hence, we get $\lambda u \in \partial J(u)$ with $\lambda = (1 - c)/\alpha(u) = J(u)/\|u\|^2$. ■

As mentioned above we can now prove that the power method decreases the energy J .

Corollary 4.9 (Energy decrease). *Let $\alpha(u) < \|u\|_*$ in (4.4). Then the iterates of Algorithm 4.1 fulfill*

$$(4.11) \quad J(u^{k+1}) \leq J(u^k),$$

with equality if and only if $\lambda u^k \in \partial J(u^k)$ for $\lambda = J(u^k)/\|u^k\|^2$.

Proof. Applying Proposition 4.8 to $u = u^k$ and $v = T(u^k)$ yields

$$J(u^{k+1}) = J\left(\frac{T(u^k)}{\|T(u^k)\|}\right) = \frac{J(T(u^k))}{\|T(u^k)\|} \leq \frac{J(u^k)}{\|u^k\|} = J(u^k),$$

where we used the absolute one-homogeneity of J and $\|u^k\| = 1$. ■

Some remarks regarding the admissible choice of $\alpha(u)$ are in order.

Remark 4.3. *For a quick algorithm one does not have to compute the dual norm $\|u\|_*$, which bounds the admissible regularization parameters $\alpha(u)$, explicitly. Instead, one can make use of the lower bound $\|u\|_* \geq \|u\|^2 / J(u)$ which was derived in Proposition 4.6.*

Remark 4.4 (Constant regularization parameter). *Of course, choosing a constant regularization parameter in (4.4), which does not depend on the previous iterate, is possible. Let to this end choose $\alpha(u) \equiv \alpha < 1/J(u^0)$ for all $u \in \mathcal{H}$. Then by Corollary 4.9 it holds that $\alpha(u^k) < 1/J(u^0) \leq 1/J(u^k)$ for any $k \in \mathbb{N}$ and hence the power method Algorithm 4.1 is well-defined according to Corollary 4.7.*

Before we can prove our main theorem, the convergence of the proximal power method, we need a lemma which studies continuity properties of the operator (4.4).

Lemma 4.10 (Continuity). *Let $(u^k) \subset \mathcal{H}$ be a sequence converging to u^* , and let $v^k := \text{prox}_{\alpha(u^k)}^J(u^k)$ for $k \in \mathbb{N}$. If the sequence of regularization parameters fulfills $\lim_{k \rightarrow \infty} \alpha(u^k) = \alpha^* > 0$ then (v^k) converges to some $v^* \in \mathcal{H}$ and it holds $v^* = \text{prox}_{\alpha^*}^J(u^*)$.*

Proof. From the optimality of v^k we deduce

$$\frac{1}{2} \|v^k - u^k\|^2 + \alpha(u^k) J(v^k) \leq \frac{1}{2} \|v - u^k\|^2 + \alpha(u^k) J(v), \quad \forall v \in \mathcal{H}.$$

Choosing $v = 0$, we can infer

$$(4.12) \quad \limsup_{k \rightarrow \infty} \frac{1}{2} \|v^k - u^k\|^2 + \alpha(u^k)J(v^k) \leq \limsup_{k \rightarrow \infty} \frac{1}{2} \|u^k\|^2 < \infty,$$

since (u^k) is a convergent sequence and hence bounded. By triangle inequality it holds

$$\|v^k\| \leq \|v^k - u^k\| + \|u^k\|$$

which together with (4.12) shows that $\limsup_{k \rightarrow \infty} \|v^k\| < \infty$. Furthermore, since we have assumed that $\lim_{k \rightarrow \infty} \alpha(u^k) = \alpha^* > 0$, we also get that $\limsup_{k \rightarrow \infty} J(v^k) < \infty$. Hence, by [Assumption 3](#) a subsequence of (v^k) converges to some $v^* \in \mathcal{H}$. Using lower semi-continuity of J and the strong convergences of (u^k) and (v^k) it holds

$$\begin{aligned} \frac{1}{2} \|v^* - u^*\|^2 + \alpha^* J(v^*) &\leq \liminf_{k \rightarrow \infty} \frac{1}{2} \|v^k - u^k\|^2 + \alpha(u^k)J(u^k) \\ &\leq \liminf_{k \rightarrow \infty} \frac{1}{2} \|v - u^k\| + \alpha(u^k)J(v) = \frac{1}{2} \|v - u^*\|^2 + \alpha^* J(v), \quad \forall v \in \mathcal{H}. \end{aligned}$$

This shows that $v^* = \text{prox}_{\alpha^*}^J(u^*)$. The same argument shows that in fact every convergent subsequence of (v^k) converges to v^* and hence the whole sequence (v^k) converges to v^* . \blacksquare

In the previous lemma we have seen that the choice of regularization parameters $\alpha(u)$ cannot be arbitrary but must be such that along a convergent sequence (u^k) also $\alpha(u^k)$ converges to some positive value. In the following, we thus fix two possible parameter choices which have this property and are feasible in practical applications.

Definition 4.11 (Parameter rules). *Let $u^0 \in \mathcal{H}$ with $\|u^0\| = 1$ and $0 < J(u^0) < \infty$, and let $c \in (0, 1)$ be a constant. We define the constant parameter rule for T given by (4.4) as*

$$(4.13) \quad \alpha(u) = \frac{c}{J(u^0)}.$$

Similarly, we define the variable parameter rule as

$$(4.14) \quad \alpha(u) = \frac{c}{J(u)}.$$

Now we are ready to prove convergence of the proximal power method using constant or variable regularization parameters.

Theorem 4.5 (Convergence of the proximal power method). *Let $(u^k) \subset \mathcal{H}$ be the sequence generated by the power method [Algorithm 4.1](#) associated to the operator $T(u) = \text{prox}_{\alpha(u)}^J(u)$ with constant or variable parameter rule. Under [Assumption 2](#) and [Assumption 3](#) a subsequence of (u^k) converges to some $u^* \in \mathcal{H} \setminus \{0\}$ which meets $\lambda u^* = T(u^*)$ for some $0 < \lambda < 1$.*

Proof. Since by assumption the sublevel sets of $\|\cdot\| + J(\cdot)$ are compact and according to [Corollary 4.9](#) sequence (u^k) fulfills

$$\sup_{k \in \mathbb{N}} \|u^k\| + J(u^k) \leq 1 + J(u^0) < \infty,$$

it admits a convergent subsequence (which we do not relabel). We denote by u^* its limit and note that it fulfills

$$\|u^*\| = 1, \quad J(u^*) \leq \liminf_{k \rightarrow \infty} J(u^k),$$

by lower semi-continuity of J . For the constant parameter rule it is trivial that $\alpha(u^k)$ converges to some positive value. Let us therefore study the variable parameter rule $\alpha(u^k) := c/J(u^k)$ with $0 < c < 1$. Then according to [Corollary 4.7](#) it holds that $\alpha(u^k)$ is an increasing sequence which is bounded by $\alpha(u^k) \leq \frac{c}{c_P}$, where c_P denotes the Poincaré-type constant from [Assumption 2](#). Hence, $\lim_{k \rightarrow \infty} \alpha(u^k) = \alpha^*$ exists and by lower semi-continuity of J one has

$$(4.15) \quad \alpha^* = \lim_{k \rightarrow \infty} \alpha(u^k) = \frac{c}{\liminf_{k \rightarrow \infty} J(u^k)} \leq \frac{c}{J(u^*)}.$$

Applying [Lemma 4.10](#) gives that $v^k := \text{prox}_{\alpha(u^k)}^J(u^k)$ converges to some $v^* \in \mathcal{H}$ and it holds $v^* = \text{prox}_{\alpha^*}^J(u^*)$. Note that (4.15) together with [Proposition 4.6](#) implies that $v^* \neq 0$.

It remains to be shown that v^* and u^* are collinear since this implies that u^* is an eigenvector. To this end, we note that by [Lemma 4.12](#) below it holds

$$\lim_{k \rightarrow \infty} \left\| \|v^k\| - \langle v^k, u^k \rangle \right\| = 0.$$

Using $v^k \rightarrow v^*$ and $u^k \rightarrow u^*$ we get $\|v^*\| = \langle v^*, u^* \rangle$ which readily implies $u^* = v^*/\|v^*\|$. Hence, we infer

$$\text{prox}_{\alpha^*}^J(u^*) = v^* = \|v^*\| u^* = \tilde{\lambda} u^*$$

with $\tilde{\lambda} := \|v^*\| > 0$. Note that $\tilde{\lambda} \leq 1$ since the proximal operator has unitary Lipschitz constant and thus meets

$$\tilde{\lambda} \|u^*\| = \|\text{prox}_{\alpha^*}^J(u^*) - \text{prox}_{\alpha^*}^J(0)\| \leq \|u^*\|.$$

Indeed, it even holds $\tilde{\lambda} < 1$ since otherwise the optimality condition

$$(4.16) \quad \frac{1 - \tilde{\lambda}}{\alpha^*} u^* \in \partial J(u^*)$$

of problem (4.2) would reduce to $0 \in \partial J(u^*)$ which means $J(u^*) = 0$. Due to $\|u^*\| = 1$ and [Assumption 2](#) this is impossible. It remains to be shown that it also holds $\lambda u^* = T(u^*) = \text{prox}_{\alpha(u^*)}^J(u^*)$ for a suitable $\lambda \in (0, 1)$. For the constant parameter rule this is trivially true with $\lambda = \tilde{\lambda}$. Otherwise, we rewrite (4.16) as $\mu u^* \in \partial J(u^*)$ where $\mu := (1 - \tilde{\lambda})/\alpha^*$. Hence, $T(u^*)$ can be explicitly computed (see [5], for instance):

$$T(u^*) = \text{prox}_{\alpha(u^*)}^J(u^*) = (1 - \alpha(u^*)\mu)_+ u^* = \lambda u^*$$

with $\lambda := (1 - \alpha(u^*)\mu)_+ \leq \tilde{\lambda} < 1$. Since $\alpha(u^*) = c/J(u^*) < \|u^*\|_*$, [Proposition 4.6](#) tells us that $\lambda > 0$. ■

Lemma 4.12 (Asymptotic collinearity). *Under the conditions of [Theorem 4.5](#) it holds*

$$(4.17) \quad \lim_{k \rightarrow \infty} \left\| v^k \right\| - \langle v^k, u^k \rangle = 0,$$

Proof. To show (4.17), we note that by definition of $v^k = \text{prox}_{\alpha(u^k)}^J(u^k)$ it holds

$$\frac{1}{2} \left\| v^k - u^k \right\|^2 + \alpha(u^k) J(v^k) \leq \frac{1}{2} \left\| v - u^k \right\|^2 + \alpha(u^k) J(v), \quad \forall v \in \mathcal{H}.$$

Choosing $v = \left\| v^k \right\| u^k$, expanding the squared norms, and using $\left\| u^k \right\| = 1$ yields

$$\frac{1}{2} \left\| v^k \right\|^2 - \langle v^k, u^k \rangle + \frac{1}{2} + \alpha(u^k) J(v^k) \leq \frac{1}{2} \left\| v^k \right\|^2 - \left\| v^k \right\| + \frac{1}{2} + \alpha(u^k) \left\| v^k \right\| J(u^k).$$

This can be simplified to

$$\left\| v^k \right\| - \langle v^k, u^k \rangle \leq \alpha(u^k) \left\| v^k \right\| \left(J(u^k) - \frac{1}{\left\| v^k \right\|} J(v^k) \right).$$

First we note $\alpha(u^k) \left\| v^k \right\|$ is uniformly bounded by some $C > 0$. This is due to the fact that $\left\| v^k \right\|$ is bounded since $v^k \rightarrow v^*$ and the estimate

$$\alpha(u^k) \leq \frac{c}{J(u^k)}$$

where $J(u^k)$ is uniformly bounded away from zero thanks to [Assumption 2](#). Using that by definition $u^{k+1} = v^k / \left\| v^k \right\|$, we obtain

$$\left\| v^k \right\| - \langle v^k, u^k \rangle \leq C \left(J(u^k) - J(u^{k+1}) \right).$$

If we sum this inequality we obtain a telescopic sum on the right hand side which is uniformly bounded. Hence, using also that the left hand side is non-negative, we obtain

$$\lim_{k \rightarrow \infty} \left\| v^k \right\| - \langle v^k, u^k \rangle = 0. \quad \blacksquare$$

4.3. Networks: A Toy Example. Here we study an extremely simple “2-pixel” network with ReLU activation function. It is shown that nonlinearity plays a crucial role in such networks, where the operating range is critical. Unlike the one-homogeneous case of previous section, applying [Algorithm 4.1](#) directly results in reaching only degenerate solutions. This motivates us in the next section to develop a range-aware algorithm, which fits better to nonlinear operators, working only within an expected range.

For the linear eigenproblem (2.5) it is clear that, by linearity, every multiple of u is an eigenvector with eigenvalue λ , as well. For nonlinear maps, such as neural nets, this is typically not the case, as the following example shows. Let us consider the map $T : \mathbb{R}^2 \rightarrow \mathbb{R}^2$, given by a simple one-layer ReLU network

$$T(u) = \text{ReLU} \left[\begin{pmatrix} -1 & 0 \\ 0 & 1 \end{pmatrix} \begin{pmatrix} u_1 \\ u_2 \end{pmatrix} + \begin{pmatrix} 1 \\ -1 \end{pmatrix} \right] = \begin{pmatrix} \max(1 - u_1, 0) \\ \max(u_2 - 1, 0) \end{pmatrix}.$$

After some calculations one easily sees that the set of eigenvectors of T consists of the four different sets with respective eigenvalues, given by

$$\begin{aligned} S_1 &= \{(\alpha, 0) : 0 < \alpha < 1\}, & \lambda_1 &= \frac{1 - \alpha}{\alpha}, \\ S_2 &= \left\{ \left(\frac{1}{1 + \alpha}, \frac{1}{1 - \alpha} \right) : 0 < \alpha < 1 \right\}, & \lambda_2 &= \alpha, \\ S_3 &= \{(\alpha, 0) : \alpha < 0\}, & \lambda_3 &= \frac{1 - \alpha}{\alpha}, \\ S_4 &= \{(u_1, u_2) : u_1 \geq 1, u_2 \leq 1\}, & \lambda_4 &= 0. \end{aligned}$$

Figure 1 shows the sets of eigenvectors. So does the simple Algorithm 4.1 manage to find eigenvectors of T ? Since by definition T only returns non-negative vectors, one can never compute the negative eigenvectors in S_3 . Furthermore, due to normalization, one can only find eigenvectors with unit norm. The only non-negative eigenvector with unit norm is $(1, 0)$, which lies in S_4 , the set of eigenvectors with eigenvalue zero, i.e., the kernel of T . Indeed, one can check that for all initializations $u^0 \notin S_4 = \ker(T)$, Algorithm 4.1 converges to $(1, 0) \in S_4$ in a finite number of steps. However, the more interesting eigenvectors in S_1 , S_2 or S_3 cannot be reached, since the simple Algorithm 4.1 ignores the “natural range” where T operates.

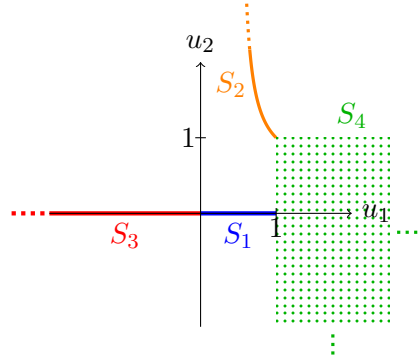


Figure 1: All eigenvectors of T . The dotted green region is the kernel.

5. Proposed Method for Range-Sensitive Operators. In the linear case, any eigenvector multiplied by a constant is an eigenvector with the same eigenvalue. In fact, for any homogeneous operator of degree $p \in [0, \infty)$ (i.e. $T(cu) = |c|^p u$), if u is an eigenvector with eigenvalue λ , so is cu , $c \in \mathbb{R}$ with eigenvalue $\lambda|c|^{p-1}$. Thus, eigenvectors are not restricted to a certain range of values. For more general nonlinear operators, however, the range of the vector is important. The operator and its respective eigenvectors may be range-sensitive. We shall now see how very common assumptions for images and denoisers yield that eigenvectors, as defined until now, exist only for unit eigenvalues. We thus later give a more relaxed definition. We discuss the finite-dimensional case $\mathcal{H} = \mathbb{R}^n$ since we aim at designing a power method for imaging / network purposes. Hence, we view the denoising network as operator $T : U \rightarrow U$, where $U \subset \mathbb{R}^n$ meets (3.1). To this end, we state two canonical assumptions on the nature of the denoising network T under consideration:

Assumption 4 (Pixels are in a specific value range). *Pixel values are in a specific predefined range, typically non-negative, and usually either $[0, 1]$ or $[0, 255]$. A nonlinear operator T stemming from a neural network is usually trained on images within a predefined range. Thus at inference unexpected results may be produced, if the input image is not in the expected range.*

Assumption 5 (Denoisers are unbiased). *Common denoisers are designed for additive white noise (either Gaussian or uniform) of expected value zero. Thus it is common that a denoiser T preserves the mean image value, which can be expressed as $\langle T(u), 1 \rangle = \langle u, 1 \rangle$.*

The second assumption severely restricts possible eigenvalues of the denoiser:

Proposition 5.1. *For any vector $u \neq 0$ with non-negative entries and a denoiser T admitting Assumption 5 above, if u is an eigenvector, as in (2.1), then $\lambda = 1$.*

Proof. If u is an eigenvector with eigenvalue λ it holds $\langle u, 1 \rangle = \langle T(u), 1 \rangle = \lambda \langle u, 1 \rangle$ due to Assumption 5. Since u has non-negative values (and is not identically zero) we know $\langle u, 1 \rangle > 0$. Hence, we can cancel $\langle u, 1 \rangle$ and obtain $\lambda = 1$. ■

Another issue is the invariance to a constant shift in illumination. We expect the behavior of T to be invariant to a small global shift in image values. That is, $T(u + c) = T(u) + c$, for any $c \in \mathbb{R}$, such that $(u + c) \in U$. We thus relax the basic eigenproblem (2.1) as follows:

$$(5.1) \quad T(u) - \overline{T(u)} = \lambda(u - \bar{u}),$$

where $\lambda \in \mathbb{R}$, $\bar{u} = \langle 1, u \rangle / |\Omega|$ is the mean value of u over the image domain Ω . Note that now (relaxed) eigenvectors, admitting (5.1), can have any eigenvalue, keeping the assumptions stated above. In addition, if u is an eigenvector, so is $u + c$, as expected for operators with invariance to global value shifts.

Associated to this adapted eigenproblem, we define a suitable Rayleigh quotient as

$$(5.2) \quad R^\dagger(u) = \frac{\langle u - \bar{u}, T(u) - \overline{T(u)} \rangle}{\|u - \bar{u}\|^2}$$

which still has the property that $\lambda = R^\dagger(u)$ whenever u fulfills the eigenvalue problem (5.1).

Remark 5.1. *A similar relaxation of the eigenvalue problem can be done for general Hilbert spaces if one replaces the mean \bar{u} by the projection onto a closed subspace and $u - \bar{u}$ by the projection onto the respective orthogonal complement. By choosing different subspaces (e.g. constant functions, affine functions, etc.) one can create different eigenvalue problems.*

Algorithm 5.1 Nonlinear Power Method for Non-Homogeneous Operators.

Input: $f \in \mathbb{R}^n$, $\varepsilon \in \mathbb{R}^+$.

1. Initialize: $u^0 \leftarrow f$, $k \leftarrow 1$.
2. Repeat until $\|u^{k+1} - u^k\| < \varepsilon$:
 - $u^{k+1} \leftarrow T(u^k)$
 - $u^{k+1} \leftarrow u^{k+1} - \overline{u^{k+1}}$
 - $u^{k+1} \leftarrow \frac{u^{k+1}}{\|u^{k+1}\|} \|u^0 - \overline{u^0}\|$
 - $u^{k+1} \leftarrow u^{k+1} + \overline{u^k}$, $k \leftarrow k + 1$.

Output: (u^*, λ^*) , where $u^* = u^k$, $\lambda^* = R^\dagger(u^*)$, with R^\dagger defined in (5.2).

The modified power method is detailed in Algorithm 5.1, aiming at computing a relaxed eigenvector (5.1) by explicitly handling the mean value and keeping the norm of the initial condition. We found this adaptation to perform well on denoising networks.

6. Numerical results.

6.1. Eigenvectors of Shallow Denoising Networks. In this section, we present experimental results for the following basic denoising networks:

$$T(u) = \begin{cases} Au & \text{Linear,} \\ \sigma(Au) & \text{ReLU,} \\ \sigma(A_2\sigma(A_1u)) & \text{AutoEncoder,} \\ \sigma(B\sigma(Cu)) & \text{ConvNet,} \end{cases} \quad u \in \mathbb{R}^n$$

where σ denotes ReLU activation and $n = 28^2 = 784$ denotes image size. The involved matrices in the **Linear**, **ReLU**, and **AutoEncoder** nets are $A \in \mathbb{R}^{n \times n}$, $A_1 \in \mathbb{R}^{f \times n}$, and $A_2 \in \mathbb{R}^{n \times f}$, where **SmallAE** and **LargeAE** denote feature space sizes $f = 25$ and $f = 200$, respectively. The convolutional layer C in **ConvNet** produces 16 kernels of size 6×4 , and the subsequent fully connected layer corresponds to a matrix $B \in \mathbb{R}^{n \times n}$. The networks were trained on 5000 pairs of noisy and clean images from the MNIST database with values in $[0, 1]$.

We use the simple [Algorithm 4.1](#) to compute eigenvectors of the net. This seems reasonable, since all nets are positively homogeneous due to the lack of bias terms. All eigenvectors computed fulfill $\|\lambda u - T(u)\| < 10^{-7}$ where $\lambda = \|T(u)\|$ denotes the eigenvalue. This means they fulfill the eigenvector relation with high numerical accuracy. The eigenvectors and corresponding eigenvalues are shown in [Figure 2](#). Furthermore, [Table 1](#) shows the Root Mean Squared Errors (RMSE) of the trained networks on an unseen test set of MNIST digits.

One should remark that the eigenvectors of the **Linear** net were computed with standard methods*, since they coincide with eigenvectors of the matrix A . Indeed, in our experiments A had several eigenvectors with real eigenvalues, but we only show the three with the largest eigenvalue. Similarly, for the other nets we show all eigenvectors that we were able to compute using different initializations of [Algorithm 4.1](#). For each network, we initialized the power method with 36 different images, being zero apart from a single pixel with varying position.

While by this method most nets only exhibit one to three different eigenvectors, the **LargeAE** net shows eleven different eigenvectors. Furthermore, some of the eigenvectors of the **Linear** and **LargeAE** nets show remarkable similarity with handwritten digits. This could indicate overfitting, which is also supported by the relatively low RMSE of these nets ([Table 1](#)). On the other hand, the **SmallAE** network, having by far the smallest number of parameters, exhibits only one eigenvector and has larger RMSE. This might indicate that this network is not very much bound to the training data and has few invariances.

Network	Linear	ReLU	SmallAE	LargeAE	ConvNet
RMSE	0.097345	0.083013	0.13968	0.097402	0.083913

Table 1: Root Mean Squared Errors of the networks on an unseen test set of MNIST digits

*We used the MATLAB routine `eig`.

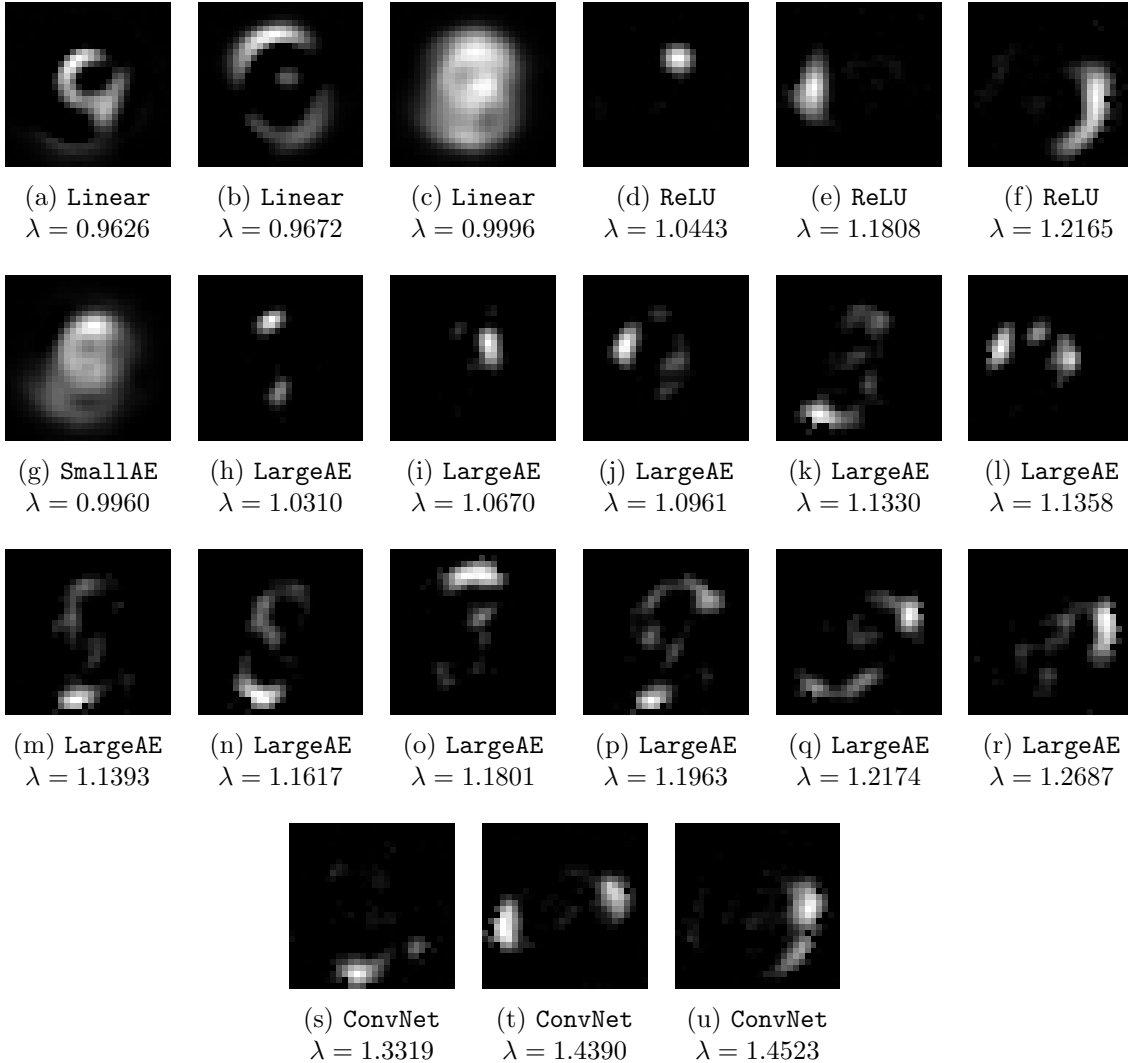


Figure 2: Eigenvectors and eigenvalues for the different shallow denoising networks. Linear eigenvectors are computed with standard methods, all others using [Algorithm 4.1](#) with different initializations.

6.2. Approximate Eigenvectors as Stable and Unstable Modes of Deep Denoising Nets.

In this section, we analyze eigenproblems for deep denoising nets. Directly applying [Algorithm 4.1](#) for these nets results in less meaningful results (cf. [Figure 3](#)), due their unique nature, as detailed in [section 5](#). Thus, we use the adapted eigenproblem [\(5.1\)](#) and [Algorithm 5.1](#).

The resulting solutions can only be regarded as approximate eigenvectors, since they do not accurately solve the eigenproblem (see [Definition 4.4](#), using degrees throughout the paper). Thus, we address these solutions as stable and unstable modes of the denoiser. Stable modes are optimal inputs for the denoiser, achieving superior PSNR in noise removal, and corresponding to large eigenvalues. We also show a method for generating unstable modes, which are strongly suppressed by the denoiser and correspond to small eigenvalues.

Figure 4 shows a known behavior of stable and unstable modes: the denoiser better removes noise from its stable modes, than from natural images. Much poorer noise removal is achieved when denoising its unstable modes, which are approximately as unstable as noise itself. We show such stable and unstable modes for the FFDnet [45] (subsection 6.2.1) and DnCNN [44] (subsection 6.2.2) deep denoising nets. Throughout our experiments, we validate these are stable modes following Definition 4.4 and Proposition 4.2 and Proposition 4.3 (see [26]). First, the Rayleigh quotient $R^\dagger(u)$ stabilizes to a value λ . Second, the angle θ between u^k and $T(u^k)$ decreases to approximately zero. Also, the eigenproblem (5.1) approximately holds for each pixel.

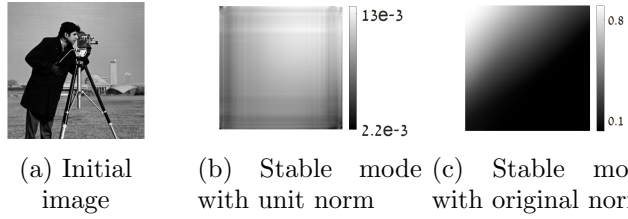
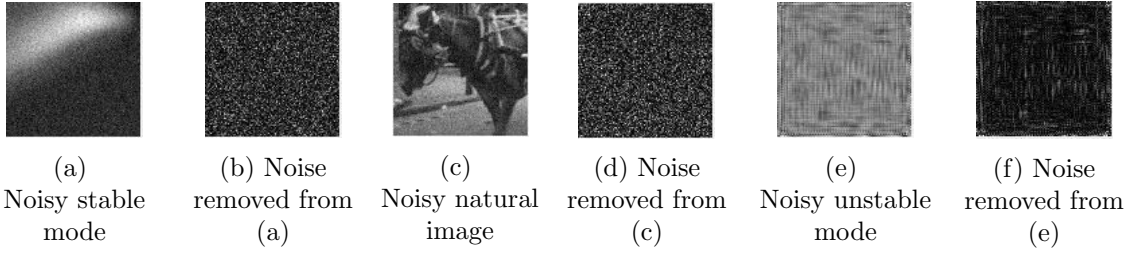
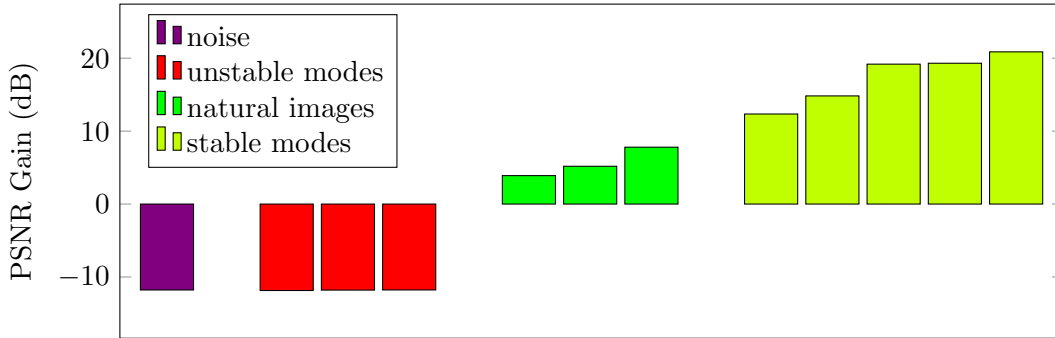


Figure 3: FFDnet’s eigenvectors using the simple power method Algorithm 4.1 (initial condition cameraman). $\langle T(u), 1 \rangle = \langle u, 1 \rangle$ holds only approximately. (b) normalizing to unit norm: $\lambda = 1.123$, $\theta_{2000} = 0^\circ$. (c) normalizing initial norm: $\lambda = 0.9999$, $\theta_{2000} = 0.56^\circ$.

Throughout our experiments, we validate these are stable modes following Definition 4.4 and Proposition 4.2 and Proposition 4.3 (see [26]). First, the Rayleigh quotient $R^\dagger(u)$ stabilizes to a value λ . Second, the angle θ between u^k and $T(u^k)$ decreases to approximately zero. Also, the eigenproblem (5.1) approximately holds for each pixel.



FFDnet Denoising - PSNR Gain



(g) PSNR gain when denoising different noisy images: stable modes vs. natural images vs. unstable modes vs. noise images. The noise variance of the noise is 1/15 of the image variance.

Figure 4: Illustration of a known property for stable and unstable modes. FFDnet achieves best denoising results for its stable modes (a-b), medium results for natural images (c-d), and worst results for unstable modes (e-f). The noise removed from the stable mode is also more uniform (note that (f) contains some structure of (e)). (g): PSNR gain when denoising using FFDnet for different noisy images (noise image result averaged over 50 images).

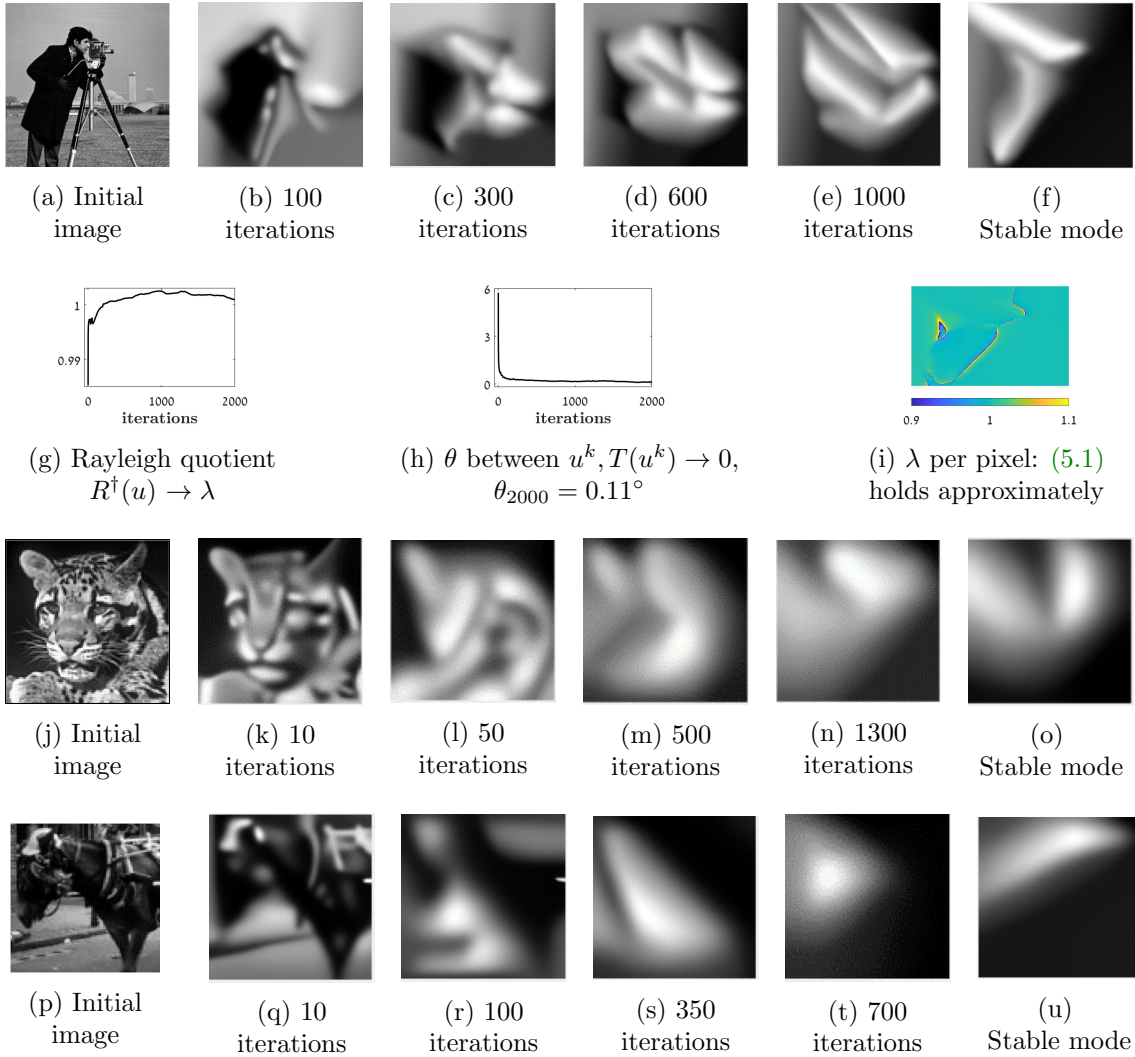


Figure 5: FFDnet power method evolution to final stable modes (2000 iterations), validated following subsection 6.2. Rows 1-2: initial condition **cameraman**, with $\lambda = 1.0009$. Row 3: initial condition **tiger**, with $\lambda = 1.0036$, $\theta_{2000} = 0.07^\circ$. Row 4: initial condition **horse**, with $\lambda = 1.0039$, $\theta_{2000} = 0^\circ$.

6.2.1. FFDnet Deep Denoising Net. We first present results of Algorithm 5.1 for the FFDnet deep denoising [45].

Nature of Operator. We demonstrate the smoothing nature of FFDnet by iterative denoising (no power method) using 500 iterations in Figure 9a.

Stable Modes. Figure 5 shows the evolution of the power method to the final stable modes, using FFDnet on three different initial images. Eigenvalues are larger than but very close to 1, which is unusual for a denoiser (see Cor. 1 in [26]). The stable modes differ from each other, each depending on its initial condition. Modes were validated following the framework detailed in subsection 6.2.

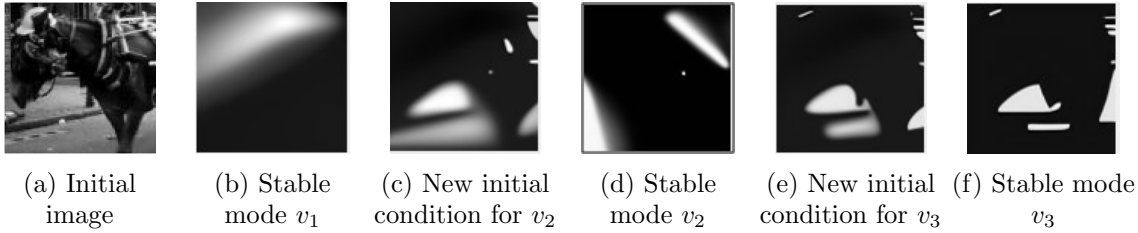


Figure 6: FFDnet further stable modes (initial condition `horse`), validated following [subsection 6.2](#). For the stable modes v_i , fifty projection iterations enforce orthogonality to modes v_j for $j < i$, generating a new initial condition. 2000 iterations of the power method then follow. (d): v_2 , with $\lambda_2 = 0.9934$, $\theta_{2000} = 0.26^\circ$. (f): v_3 , with $\lambda_3 = 0.9815$, $\theta_{2000} = 0.09^\circ$.

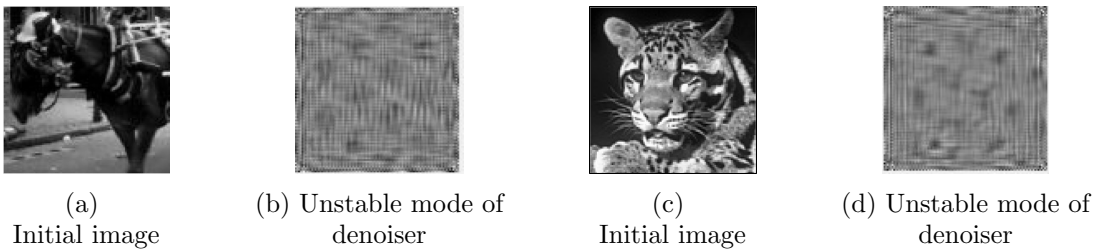


Figure 7: Stable modes of the FFDnet texture generator using 10000 iterations, validated following [subsection 6.2](#). These are *unstable* modes of the FFDnet denoiser. (a)-(b): initial condition `horse`, with $\lambda = 1.006$, $\theta_{10000} = 0.23^\circ$. (c)-(d): initial condition `tiger`, with $\lambda = 1.0033$, $\theta_{10000} = 0.4829^\circ$.

Further Stable Modes. [Figure 6](#) shows further stable modes using FFDnet with initial condition `horse`. We here follow the concept introduced in Algorithm 4 in [\[26\]](#). Given previously attained stable modes, we first perform a small number of power iterations with projections onto the space orthogonal to these modes, to ensure sufficient deviation and avoid recurrence of stable modes. We then perform the regular nonlinear power method to reach a state which meets [\(5.1\)](#). Eigenvalues are now smaller than but very close to 1, as expected from a denoiser (see Cor. 1 in [\[26\]](#)). In this example, the eigenvalues meet $\lambda_1 > \lambda_2 > \lambda_3$, but this cannot be guaranteed in general.

Unstable Modes. We follow Section 2.6 in [\[26\]](#) to reveal unstable modes of the denoiser. We construct the complementary texture generator operator, $T^\dagger(u) := u - T(u)$. [Figure 7](#) shows stable modes of T^\dagger , with eigenvalues very close to but larger than 1. Modes were validated following [subsection 6.2](#). Note that stable modes of T^\dagger are unstable modes of the denoising net T , characterized by fine textures.

Robustness to Small Degradations. [Figure 8](#) illustrates the robustness of stable modes to small degradations. A degraded stable mode has a similar Rayleigh quotient to that of the original stable mode. When applying the power method, it evolves back to the critical point in its neighborhood, given by the original stable mode. We also show how noise robustness holds in a very wide sense. The denoiser considers textures and fine details, such as the small eigenvector, as noise to be removed. On the other hand, the texture generator prefers noise and textures and it considers coarse structures as noise to be removed.

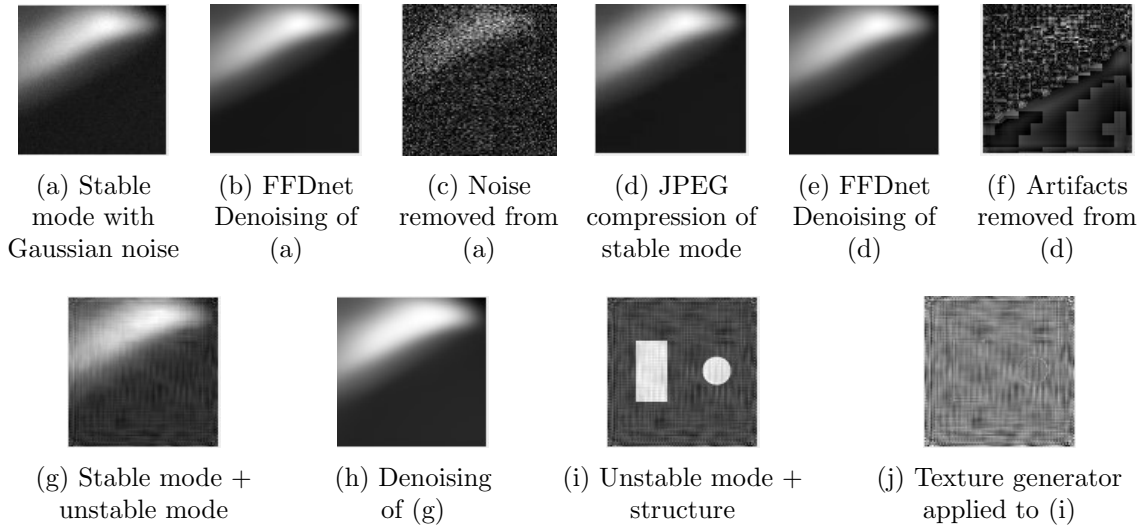


Figure 8: Robustness of FFDnet’s stable mode to small degradations. (a)-(c): noise degradation with variance 0.01^2 corrected by 10 power iterations. (d)-(f): JPEG compression degradation, corrected by 10 power iterations. (g)-(h): The unstable mode is considered as “noise” by the denoiser. (i)-(j): A structure is considered as “noise” by the texture generator.

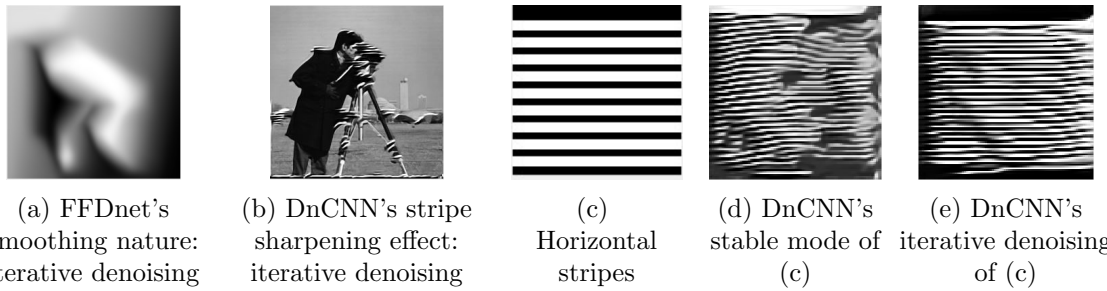


Figure 9: Nature of FFDnet and DnCNN. (a-b) 500 iterations of iterative denoising (no power method) of *cameraman*: FFDnet’s smoothing nature (a) vs. DnCNN’s stripe sharpening effect (b). (c)-(e): DnCNN “prefers” stripes: iterative denoising.

6.2.2. DnCNN Deep Denoising Net. We present results of [Algorithm 5.1](#) for the DnCNN deep denoising net [44].

Nature of Operator. Although it is a smoothing operator, DnCNN also produces a sharpening effect, adding stripes to the image. We first illustrate in [Figure 9b](#) the horizontal stripes produced by iterative DnCNN denoising of the *cameraman* image, using 500 iterations. We also show the stable mode after 5000 iterations of the power method and iterative denoising result after 500 iterations for an artificial stripe image. Even after a single application of DnCNN, $u, T(u)$ are already almost collinear, demonstrating this net’s tendency to stripes. Further experiments showed that this is true for stripes of different orientations. DnCNN is a *blind* denoiser that deals with unknown noise level, but assumes that noise is present in the input. Hence we believe the sharpening effect is caused by applying DnCNN iteratively throughout the power iterations to *noiseless* and smooth images, for which it was not trained.

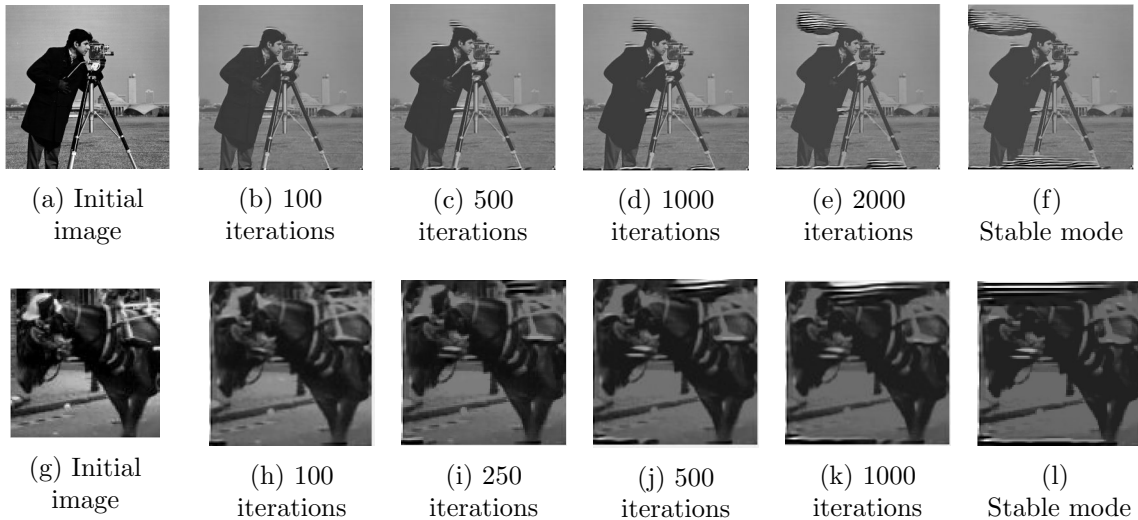


Figure 10: DnCNN power method evolution to final stable modes after 5000 iterations, validated following [subsection 6.2](#). Row 1: initial condition `cameraman`, with $\lambda = 1.0024$, $\theta_{2000} = 0.13^\circ$. Row 2: initial condition `horse`, with $\lambda = 1.0054$, $\theta_{2000} = 0.24^\circ$.

Stable Modes. [Figure 10](#) shows the power method evolution to the final stable mode, using DnCNN on two different initial images. As for FFDnet, eigenvalues are larger than but very close to 1. The stable modes mainly are smoothed versions of the initial conditions with additional horizontal stripes.

7. Conclusion. In this work we propose and analyze power method to compute eigenvectors of proximal operators and neural networks. For proximal operators of one-homogeneous functionals we prove that a straightforward generalization of the linear power method converges to eigenvectors. However, general denoising neural networks require a more general algorithm, which takes their natural domain into account. Despite the lack of theoretical convergence guarantees, this algorithm yields satisfactory approximate eigenvectors of the networks, which we interpret as (un)stable modes.

Future work will include investigating network architectures for which one can provably compute eigenvectors. Closely related to this is the design of 1-Lipschitz (non-expansive) networks, which are natural candidates for studying eigenvectors and fixed points. A possible future application of (un)stable modes or eigenvectors of a network might consist in designing indicators for the amount of over-fitting, or for the generalization ability, respectively.

Acknowledgments. This work was supported by the European Union’s Horizon 2020 research and innovation programme under the Marie Skłodowska-Curie grant agreement No 777826. GG acknowledges support by the Israel Science Foundation (Grant No. 534/19) and by the Ollendorff Minerva Center.

REFERENCES

- [1] J.-F. AUJOL, G. GILBOA, AND N. PAPADAKIS, *Theoretical analysis of flows estimating eigenfunctions of one-homogeneous functionals*, SIAM Journal on Imaging Sciences, 11 (2018), pp. 1416–1440.
- [2] A. I. AVILES-RIVERO, N. PAPADAKIS, R. LI, S. M. ALSALEH, R. T. TAN, AND C.-B. SCHONLIEB, *Beyond supervised classification: Extreme minimal supervision with the graph 1-laplacian*, arXiv preprint arXiv:1906.08635, (2019).
- [3] H. H. BAUSCHKE, P. L. COMBETTES, ET AL., *Convex analysis and monotone operator theory in Hilbert spaces*, vol. 408, Springer, 2011.
- [4] G. BELLETTINI, V. CASELLES, AND M. NOVAGA, *The total variation flow in \mathbb{R}^n* , Journal of Differential Equations, 184 (2002), pp. 475–525.
- [5] M. BENNING AND M. BURGER, *Ground states and singular vectors of convex variational regularization methods*, Methods and Applications of Analysis, 20 (2013), pp. 295–334.
- [6] K. BREDIES, K. KUNISCH, AND T. POCK, *Total generalized variation*, SIAM Journal on Imaging Sciences, 3 (2010), pp. 492–526.
- [7] L. BUNGERT AND M. BURGER, *Asymptotic profiles of nonlinear homogeneous evolution equations of gradient flow type*, Journal of Evolution Equations, (2019), pp. 1–32.
- [8] L. BUNGERT AND M. BURGER, *Solution paths of variational regularization methods for inverse problems*, Inverse Problems, 35 (2019), p. 105012.
- [9] L. BUNGERT, M. BURGER, A. CHAMBOLLE, AND M. NOVAGA, *Nonlinear spectral decompositions by gradient flows of one-homogeneous functionals*, To appear in Analysis & PDE, (2019).
- [10] L. BUNGERT, M. BURGER, AND D. TENBRINCK, *Computing nonlinear eigenfunctions via gradient flow extinction*, in International Conference on Scale Space and Variational Methods in Computer Vision, Springer, 2019, pp. 291–302.
- [11] L. BUNGERT, Y. KOROLEV, AND M. BURGER, *Structural analysis of an l -infinity variational problem and relations to distance functions*, arXiv preprint arXiv:2001.07411, (2020).
- [12] M. BURGER, G. GILBOA, M. MOELLER, L. ECKARDT, AND D. CREMERS, *Spectral decompositions using one-homogeneous functionals*, SIAM Journal on Imaging Sciences, 9 (2016), pp. 1374–1408.
- [13] M. BURGER AND S. OSHER, *A guide to the tv zoo*, in Level set and PDE based reconstruction methods in imaging, Springer, 2013, pp. 1–70.
- [14] T. Q. CHEN, Y. RUBANOVA, J. BETTENCOURT, AND D. K. DUVENAUD, *Neural ordinary differential equations*, in Advances in neural information processing systems, 2018, pp. 6571–6583.
- [15] I. COHEN AND G. GILBOA, *Energy dissipating flows for solving nonlinear eigenpair problems*, Journal of Computational Physics, 375 (2018), pp. 1138–1158.
- [16] I. COHEN AND G. GILBOA, *Introducing the p -laplacian spectra*, Signal Processing, 167 (2020), p. 107281.
- [17] S. DITTMER, J. EMILY, AND P. MAASS, *Singular values for relu layers*, IEEE transactions on neural networks and learning systems, (2019).
- [18] M. EGMONT-PETERSEN, D. DE RIDDER, AND H. HANDELS, *Image processing with neural networks—a review*, Pattern recognition, 35 (2002), pp. 2279–2301.
- [19] J. FAN, W. XU, Y. WU, AND Y. GONG, *Human tracking using convolutional neural networks*, IEEE Transactions on Neural Networks, 21 (2010), pp. 1610–1623.
- [20] T. FELD, J.-F. AUJOL, G. GILBOA, AND N. PAPADAKIS, *Rayleigh quotient minimization for absolutely one-homogeneous functionals*, Inverse Problems, 35 (2019), p. 064003.
- [21] R. GARG, V. K. BG, G. CARNEIRO, AND I. REID, *Unsupervised CNN for single view depth estimation: Geometry to the rescue*, in European Conference on Computer Vision, Springer, 2016, pp. 740–756.
- [22] G. GILBOA, *A spectral approach to total variation*, in International Conference on Scale Space and Variational Methods in Computer Vision, Springer, 2013, pp. 36–47.
- [23] G. GILBOA, *A total variation spectral framework for scale and texture analysis*, SIAM Journal on Imaging Sciences, 7 (2014), pp. 1937–1961.
- [24] E. HABER AND L. RUTHOTTO, *Stable architectures for deep neural networks*, Inverse Problems, 34 (2017), p. 014004.
- [25] E. HAIT AND G. GILBOA, *Spectral total-variation local scale signatures for image manipulation and fusion*, IEEE Transactions on Image Processing, 28 (2019), pp. 880–895.
- [26] E. HAIT-FRAENKEL AND G. GILBOA, *Numeric solutions of eigenvalue problems for generic nonlinear*

- operators*, arXiv preprint arXiv:1909.12775, (2019).
- [27] M. HEIN AND T. BÜHLER, *An inverse power method for nonlinear eigenproblems with applications in 1-spectral clustering and sparse pca*, in Advances in Neural Information Processing Systems (NIPS'10), 2010, pp. 847–855.
 - [28] M. HEIN AND T. BÜHLER, *An inverse power method for nonlinear eigenproblems with applications in 1-spectral clustering and sparse pca*, in Advances in Neural Information Processing Systems, 2010, pp. 847–855.
 - [29] R. A. HORN AND C. R. JOHNSON, *Matrix analysis*, Cambridge university press, 2012.
 - [30] F. LIU, C. SHEN, AND G. LIN, *Deep convolutional neural fields for depth estimation from a single image*, in Proceedings of the IEEE conference on computer vision and pattern recognition, 2015, pp. 5162–5170.
 - [31] S. MALLAT, *Understanding deep convolutional networks*, Philosophical Transactions of the Royal Society A: Mathematical, Physical and Engineering Sciences, 374 (2016), p. 20150203.
 - [32] Y. MEYER, *Oscillating patterns in image processing and in some nonlinear evolution equations*, March 2001. The 15th Dean Jacqueline B. Lewis Memorial Lectures.
 - [33] R. MISES AND H. POLLACZEK-GEIRINGER, *Praktische verfahren der gleichungsauflösung.*, ZAMM-Journal of Applied Mathematics and Mechanics/Zeitschrift für Angewandte Mathematik und Mechanik, 9 (1929), pp. 152–164.
 - [34] M. MOELLER, J. DIEBOLD, G. GILBOA, AND D. CREMERS, *Learning nonlinear spectral filters for color image reconstruction*, in Proceedings of the IEEE International Conference on Computer Vision (ICCV'15), 2015, pp. 289–297.
 - [35] H. NAM AND B. HAN, *Learning multi-domain convolutional neural networks for visual tracking*, in Proceedings of the IEEE conference on computer vision and pattern recognition, 2016, pp. 4293–4302.
 - [36] R. Z. NOSSEK AND G. GILBOA, *Flows generating nonlinear eigenfunctions*, Journal of Scientific Computing, 75 (2018), pp. 859–888.
 - [37] V. POPYAN, Y. ROMANO, J. SULAM, AND M. ELAD, *Theoretical foundations of deep learning via sparse representations: A multilayer sparse model and its connection to convolutional neural networks*, IEEE Signal Processing Magazine, 35 (2018), pp. 72–89.
 - [38] L. I. RUDIN, S. OSHER, AND E. FATEMI, *Nonlinear total variation based noise removal algorithms*, Physica D: nonlinear phenomena, 60 (1992), pp. 259–268.
 - [39] E. K. RYU, J. LIU, S. WANG, X. CHEN, Z. WANG, AND W. YIN, *Plug-and-play methods provably converge with properly trained denoisers*, arXiv preprint arXiv:1905.05406, (2019).
 - [40] J. SCHMIDHUBER, *Deep learning in neural networks: An overview*, Neural networks, 61 (2015), pp. 85–117.
 - [41] A. SZLAM AND X. BRESSON, *Total variation and Cheeger cuts*, in International Conference on Machine Learning (ICML'10), 2010, pp. 1039–1046.
 - [42] M. THORPE AND Y. VAN GENNIP, *Deep limits of residual neural networks*, arXiv preprint arXiv:1810.11741, (2018).
 - [43] L. ZEUNE, G. VAN DALUM, L. W. TERSTAPPEN, S. VAN GILS, AND C. BRUNE, *Multiscale segmentation via Bregman distances and nonlinear spectral analysis*, SIAM journal on imaging sciences, 10 (2017), pp. 111–146.
 - [44] K. ZHANG, W. ZUO, Y. CHEN, D. MENG, AND L. ZHANG, *Beyond a gaussian denoiser: Residual learning of deep CNN for image denoising*, IEEE Transactions on Image Processing, 26 (2017), pp. 3142–3155.
 - [45] K. ZHANG, W. ZUO, AND L. ZHANG, *FFDNet: Toward a fast and flexible solution for CNN-based image denoising*, IEEE Transactions on Image Processing, 27 (2018), pp. 4608–4622.
 - [46] Z. ZHANG, *Polyhedron under linear transformations*, arXiv preprint arXiv:1201.6584, (2012).